Constraints on Supersymmetric Dark Matter for Heavy Scalar Superpartners

Peisi Huang[a,d,e], **Roger A. Roglans**[c], **Daniel D. Spiegel**[c]
Yitian Sun[c], **and Carlos E.M. Wagner**[a,b,d]

[a]*Enrico Fermi Institute* & [b]*Kavli Institute for Cosmological Physics,*
[c]*University of Chicago, Chicago, IL 60637*
[d]*HEP Division, Argonne National Laboratory, 9700 Cass Ave., Argonne, IL 60439*
[e]*Physics and Astronomy Department, Texas A&M University, College Station, TX 77843*

We study the constraints on neutralino dark matter in minimal low energy supersymmetry models and the case of heavy lepton and quark scalar superpartners. For values of the Higgsino and gaugino mass parameters of the order of the weak scale, direct detection experiments are already putting strong bounds on models in which the dominant interactions between the dark matter candidates and nuclei are governed by Higgs boson exchange processes, particularly for positive values of the Higgsino mass parameter μ. For negative values of μ, there can be destructive interference between the amplitudes associated with the exchange of the standard CP-even Higgs boson and the exchange of the non-standard one. This leads to specific regions of parameter space which are consistent with the current experimental constraints and a thermal origin of the observed relic density. In this article we study the current experimental constraints on these scenarios, as well as the future experimental probes, using a combination of direct and indirect dark matter detection and heavy Higgs and electroweakino searches at hadron colliders.

I Introduction

Since its proposal in 1933 by Fritz Zwicky [1], the existence of dark matter (DM) has been supported by many indirect detection measurements. Besides observations of galaxy clusters and the magnitude of gravitational lensing, the rotation curves of spiral galaxies provide evidence that a significant portion of these galaxies is made of nonluminous matter [2, 3]. Recently, the density of cold dark matter in the universe was estimated by the Planck collaboration to be $\Omega_c h^2 = 0.1198 \pm 0.0015$ [4]. Overall, the evidence indicates that a significant portion of matter in the universe is non-baryonic, but the exact nature of dark matter is still unknown. One favored dark matter candidate is a weakly interacting massive particle (WIMP)—an uncharged, colorless, stable particle with a heavy enough mass to cease annihilation in the early stages of the universe, thus leaving behind the substantial cosmological abundance seen today [5]. No particles in the Standard Model (SM) account for all these properties, so we are forced to look at theories of physics beyond the SM (BSM).

Supersymmetry (SUSY) provides a well-motivated extension of the standard model that contains such a WIMP in the form of the lightest supersymmetric particle (LSP) [6]. In the Minimal Supersymmetric Standard Model (MSSM) with R-parity conservation, the LSP is typically the lightest neutralino $\widetilde{\chi}_1^0$.

Searches for BSM particles at the LHC have not been fruitful, and these searches put constraints on supersymmetric models. In certain models, the LHC searches now limit the mass of gluinos and the first two generations of squarks to be above 1.5 TeV [7, 8]. Other production analyses have constrained chargino and neutralino masses to be at least of the order of 100 GeV [9, 10], complementing the existing bounds from LEP2 searches (see, for example, Ref. [11]). In addition, searches for heavy Higgs bosons constrain MSSM parameters such as $\tan\beta$ and M_A, the mass of the CP-odd Higgs boson [12].

Direct dark matter detection experiments (DDMD), such as LUX [13], PICO [14], XENON100 [15], and PandaX [16], have also so far come up empty-handed. These experiments set upper bounds on both the spin-dependent (SD) and spin-independent (SI) cross sections of WIMPs scattering off nucleons. LUX presents the strongest bounds—their most recent data limits the WIMP-nucleon spin independent cross section σ_{SI} to be lower than a few times 10^{-10} pb for a WIMP of mass in the range 20 GeV $\lesssim m_\chi \lesssim$ 200 GeV [13]. Future DDMD experiment such as LZ [17] and Xenon1T [18] will probe regions of SI cross sections

two orders of magnitude lower than those probed at present, and therefore it is interesting to explore the implications of the (non)observation of a signal in these experiments.

Cheung et. al. [19] have identified regions of interest in the M_1 (bino mass), M_2 (wino mass), and μ (higgsino mass) parameter space called "blind spots", where the SI or SD cross sections are suppressed due to vanishing couplings of the LSP to the lightest CP-even Higgs and to the Z boson [19]. They worked in the decoupling regime, for very large values of the heavy Higgs boson masses, squarks, and sleptons such that they no longer affect properties relevant to DM. For smaller values of the heavy Higgs boson masses, and negative values of μ, there is in general a destructive interference between the contributions to the SI cross section amplitude coming from the exchange of the standard CP-even Higgs boson and the non-standard one. This leads to a cancellation in the total SI cross section amplitude in certain regions of parameters. This effect was first noticed numerically, while performing a scan over the MSSM parameter space [20–26]. In Ref. [27], an analytical expression for the relation between different parameters necessary to reach these generalized blind spot scenarios was presented. The present DDMD constraints are still relatively weak and allow for a wide range of parameters, which can significantly deviate from the ones associated with the blind spot scenario. However, as we will discuss in this article, if future DDMD experiments continue to strengthen these constraints, it will become necessary to consider regions of parameter space close to the blind spot scenarios.

In this paper, we explore the current constraints on these scenarios, putting emphasis on regions of parameters consistent with the observed thermal relic density, and checking these regions against DDMD, Higgs and BSM searches at the LHC. In section II, we discuss the theoretical basis and give an analytical formula for the generalized blind spot scenario. In section III, we analyze the regions in the $\mu - M_1$ parameter space allowed by SI direct detection bounds and relic density considerations. In section IV, we test these regions against searches at the LHC for electroweakinos and heavy Higgs bosons. We also discuss the constraints coming from SD and indirect dark matter detection experiments, as well as from precision measurements of the observed standard model Higgs. We reserve section V for our conclusions.

II DDMD and Blind spots

In the MSSM, assuming heavy squarks and sleptons, the neutralino SI scattering process is mediated by the exchange of CP-even Higgs bosons. For Higgsino and gaugino mass parameters of the order of the weak scale the typical SI scattering cross section through the 125 GeV Higgs boson is of the order 10^{-45} cm^2, which is in tension with the LUX results [13]. A possible way to suppress the SI scattering cross section is to decouple the heavy Higgs boson and suppress the lightest neutralino coupling to the 125 GeV Higgs boson. In the decoupling limit, the lightest and heaviest CP-even Higgs bosons in the MSSM, h and H, are given by

$$\begin{aligned} \sqrt{2}h &= \cos\beta H_d^0 + \sin\beta H_u^0 \\ \sqrt{2}H &= \sin\beta H_d^0 - \cos\beta H_u^0 \end{aligned} \tag{1}$$

where H_u^0 and H_d^0 are the real components of the neutral Higgs bosons that couple to the up and down quarks, respectively, and $\tan\beta = v_u/v_d$ is the ratio of the Higgs vacuum expectation values. Given the neutralino mass and interactions terms,

$$\begin{aligned} \mathcal{L} \supset &-\sqrt{2}g'Y_{H_u}\tilde{B}\tilde{H}_u H_u^* - \sqrt{2}g\tilde{W}^a\tilde{H}_u t^a H_u^* + (u \leftrightarrow d) + h.c. \\ &- \left(\frac{M_1}{2}\tilde{B}\tilde{B} + \frac{M_2}{2}\tilde{W}^a\tilde{W}^a + \mu\tilde{H}_d\tilde{H}_u + h.c.\right) \end{aligned} \tag{2}$$

where Y_i is the H_i hypercharge, $\tilde{B}$ and $\tilde{W}$ are the superpartners of the neutral hypercharge (Bino) and weak gauge bosons (Winos), $\tilde{H}_i$ are the superpartners of the Higgs bosons (Higgsinos), $M_{1,2}$ denote the Bino and neutral Wino mass parameters and μ is the Higgsino mass parameter. One can show that the neutralino coupling to the lightest Higgs vanishes when

$$m_\chi + \mu\sin 2\beta = 0, \tag{3}$$

where m_χ is the mass of the lightest neutralino. Under the above conditions, for very large values of the heavy Higgs boson masses, the tree-level contribution to the SI scattering cross section vanishes, which is identified as a blind spot in direct detection experiments [19].

Another way to suppress the SI scattering cross section, when the heavy Higgs is not too heavy, is to have destructive interference between the 125 GeV Higgs exchange and the heavy Higgs exchange amplitudes. In this case, one goes away from the decoupling limit and

the CP-even Higgs mixing angle may no longer be identified with β. However, the deviations of the mixing angle from the decoupling values tend to be small in the region of parameters of interest for this paper, and therefore, for simplicity we will keep the expressions valid close to the decoupling limit. In such a case, the amplitude of the scattering cross section of down-quarks to neutralinos is proportional to

$$a_d \sim \frac{m_d}{\cos\beta}\left(\frac{\cos\beta\ g_{\chi\chi h}}{m_h^2} + \frac{\sin\beta\ g_{\chi\chi H}}{m_H^2}\right), \tag{4}$$

where m_h and m_H are the masses of the lightest and heavy CP-even Higgs bosons, respectively, and $g_{\chi\chi h}$ and $g_{\chi\chi H}$ are their couplings to the lightest neutralino. In general, the coupling of the neutralinos to the heavy and light Higgs bosons are similar in magnitude, and they may differ in sign. The heavy Higgs contribution, although suppressed by the square of m_H is enhanced by $\tan\beta$. Therefore, for moderate or large values of $\tan\beta$ the light and heavy Higgs contributions to the amplitude may be similar in magnitude and may interfere destructively.

Taking into account also the interaction of neutralinos with up-quarks in order to define the neutralino interaction with nuclei, one can show that the SI scattering cross section is proportional to [27]

$$\sigma_p^{SI} \sim \left[(F_d^{(p)} + F_u^{(p)})(m_\chi + \mu\sin 2\beta)\frac{1}{m_h^2} + \mu\tan\beta\cos 2\beta(-F_d^{(p)} + F_u^{(p)}/\tan^2\beta)\frac{1}{m_H^2}\right]^2, \tag{5}$$

with $F_u^{(p)} \approx 0.15$ and $F_d^{(p)} \approx 0.14$. The first term denotes the contribution of the lightest Higgs and its cancellation leads to the traditional blind spot scenarios discussed above [19]. The second term is the contribution of the heavy Higgs and as mentioned before for values of $|\mu| \gtrsim m_\chi$ and large $\tan\beta$ may become of the same order as the SM-like Higgs one.

For moderate or large values of $\tan\beta$, the tree-level contribution, mediated by the CP-even Higgs bosons, vanishes when [27]

$$2(m_\chi + \mu\sin 2\beta)\frac{1}{m_h^2} \simeq -\mu\tan\beta\frac{1}{m_H^2}. \tag{6}$$

Eq. (6) defines what we call a generalized blind spot in direct dark matter detection experiments. It is clear from this expression that the blind spot scenario demands $\mu < 0$. Considering the case of heavy gluinos and scalar superpartners of the quarks and leptons, and assuming that the wino is significantly heavier than the bino (in practice we will assume the relation implied by gaugino mass unification, $M_2 \simeq 2M_1$), the generalized blind

spot scenario can accommodate the right relic density in the well-tempered region [28], in which $M_1 \simeq |\mu|$, as well as the A-funnel region, in which $M_A \simeq 2m_{\tilde{\chi}_1^0}$ and the proper relic density [4, 29] is obtained through resonant annihilation with the heavy Higgs bosons. In this article we shall not analyze the case of wino-bino mixed dark matter that demands a high degree of degeneracy of the gaugino masses, $M_2 \simeq M_1$, and that leads to an extra suppression of the spin independent DDMD cross section due to the small Higgsino component of the dark matter candidates. For details of this case, see Ref. [30]. In addition to Eq. (6), pure Higgsino or gaugino states, also lead to a large suppression to the DDMD (see, for instance Ref. [31] and [32]). In this work, we will concentrate on the region where $M_1 < M_2$, in which the thermal relic density can be naturally obtained for $m_{\tilde{\chi}_1^0}$ of the order of weak scale.

III   Direct Dark Matter Detection Constraints
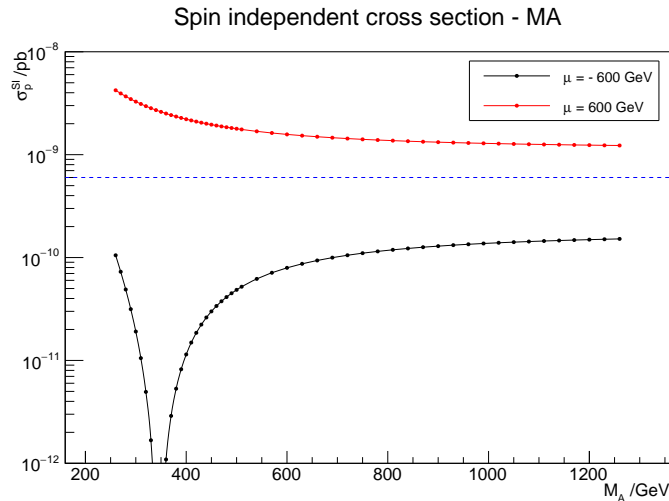
A.   Allowed Parameter Space

Figure. 1: Spin independent scattering cross section for fixed $\tan \beta = 7$, $|\mu| = 600$ GeV, $M_1 = 400$ GeV. The black line is for $\mu < 0$ and the red line is for $\mu > 0$. The blue dashed line represents the LUX 2016 constraint for $m_\chi = 400$ GeV. As M_A increases the heavy Higgs becomes decoupled from the LSP, and σ_p^{SI} approaches an asymptotic value. Note that the asymptotic value is significantly greater for $\mu > 0$ than for $\mu < 0$. When experimental limits drop below the asymptotic value of the $\mu < 0$ branch, an upper bound and a lower bound on M_A will be present, and we are forced closer to the blind spot.

The expression of the SI cross section, Eq. (5), shows that, in general, the light Higgs and heavy Higgs contributions interfere destructively (constructively) for negative (positive)

values of μ. For negative μ, scattering cross sections below the present LUX bounds are achievable even when the heavy Higgs boson is decoupled from the LSP as negative values of μ lead to a suppression in the neutralino Higgs coupling. For instance, for $\tan\beta = 7$, $\mu = \pm 600$ GeV, and $M_1 = 400$ GeV, Fig. 1 demonstrates that the scattering cross section may approach a relatively low asymptotic value in the limit $M_A \to \infty$ where the heavy Higgs is decoupled. The present LUX bound for $m_\chi \simeq M_1 = 400$ GeV is approximately $\sigma_p^{\rm SI} < 5 \times 10^{-10}$ pb [13], so for the example in Fig. 1 all cross section values obtained for $\mu > 0$ are excluded. To quantify how much a particular point in the $\mu - M_1$ plane is excluded, we compute the minimal value of M_A consistent with current LUX bound [13] in Fig. 2. In the red region, the lower bound on M_A tends to infinity, indicating that the particular point is excluded for all M_A. In applying the LUX bounds, we have implicitly assumed that the right relic density is obtained in all the parameter space, which could, for instance, demand a non-thermal contribution in large regions of parameter [33]. However, the exclusion region covers the entirety of the well-tempered region $M_1 \simeq \mu$ [34], and one can only obtain the correct relic density via heavy Higgs mediated resonant annihilation near the blue region. We will comment on this case later, but since the SI cross section is in tension with the current LUX bound in the majority of region consistent with a observed thermal dark matter relic density, we shall focus our attention on the $\mu < 0$ case.

For the $\mu < 0$ case, and assuming again the proper relic density in the whole parameter space, we compute the maximal value of M_A consistent with current spin independent DDMD bounds in order to quantify the need for a destructive interference to reduce $\sigma_p^{\rm SI}$ for the $\mu < 0$ case. Fig. 3 shows that, contrary to the $\mu > 0$ case, the present LUX bounds [13] only constrain the value of M_A away from the decoupling limit close to the well-tempered region $M_1 \simeq |\mu|$, or for $|\mu| \ll M_1$.

If one assumed a thermal origin of the relic density, then the above constraints would be modified. In the upper left region of the plot, the thermal neutralino dark matter is under-abundant (see Fig. 6 for the thermal relic density), so we assume there is another component, for instance, the axions, that contributes to the relic density. In this case, the LUX bound should be rescaled according to the thermal relic density of $\tilde{\chi}_1^0$, thereby relaxing the upper bound on M_A, as shown in Fig. 4. The proper relic density may be obtained thermally in the well-tempered region (inside the white dashed band in Fig. 3), for which LUX imposes an upper bound on M_A. This upper bound is of order of 350 GeV or smaller
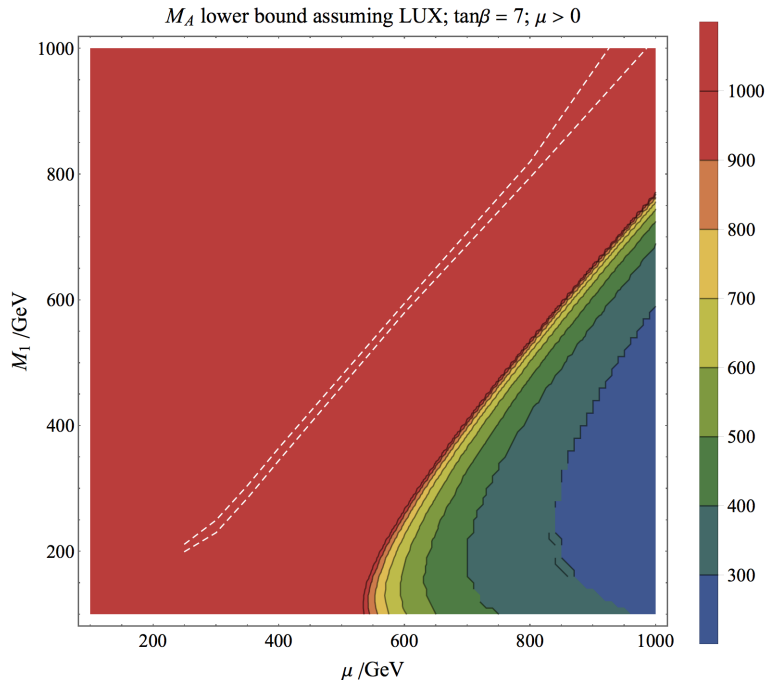
Figure. 2: Lower bounds on M_A due to 2016 LUX bounds for $\mu > 0$, assuming the observed relic density in the whole parameter space. The value of M_A is chosen to be at the minimum value allowed by the LUX bound, and is indicated by the color scale. In cases where the SI cross section is not allowed for all values of M_A, the lower bound is marked as infinity, corresponding to the red color. The region between the white dashed lines represents the well-tempered region, with the relic densities that differ from the observed value by less than 20%. It can be seen that the well-tempered region is completely excluded. However, near the blue region away from the well-tempered region, the correct thermal relic density may still be achieved by resonant annihilation.

for $\tan\beta = 7$ and large values of the neutralino mass. However, it raises to values of order 400 GeV for neutralino masses of the order of 300 GeV.

The proper thermal relic density may be also obtained to the right of the well-tempered region, in the so-called A-funnel region, by setting $M_A \simeq 2m_{\tilde{\chi}_1^0}$ such that the heavy Higgses mediate the resonant annihilation of the LSP, reducing the relic density to the correct value. Thus, points in the parameter space are allowed by LUX and relic density consideration when the upper bound on M_A is larger than or on the order of $2m_{\tilde{\chi}_1^0}$, corresponding to the blue and green regions in Fig. 3 with $M_1 < |\mu|$. For sufficiently small values of M_1 the value of the amplitude due to the exchange of the heavy CP-even Higgs may be sufficiently large to induce an increase of the cross section toward values restricted by LUX, as seen on the left of Fig. 1. As we will show below, this situation only occurs for very small values of M_1. Larger values of M_1, of the order of the weak scale, would only be restricted if future SI DDMD experiments fail to see a signal.
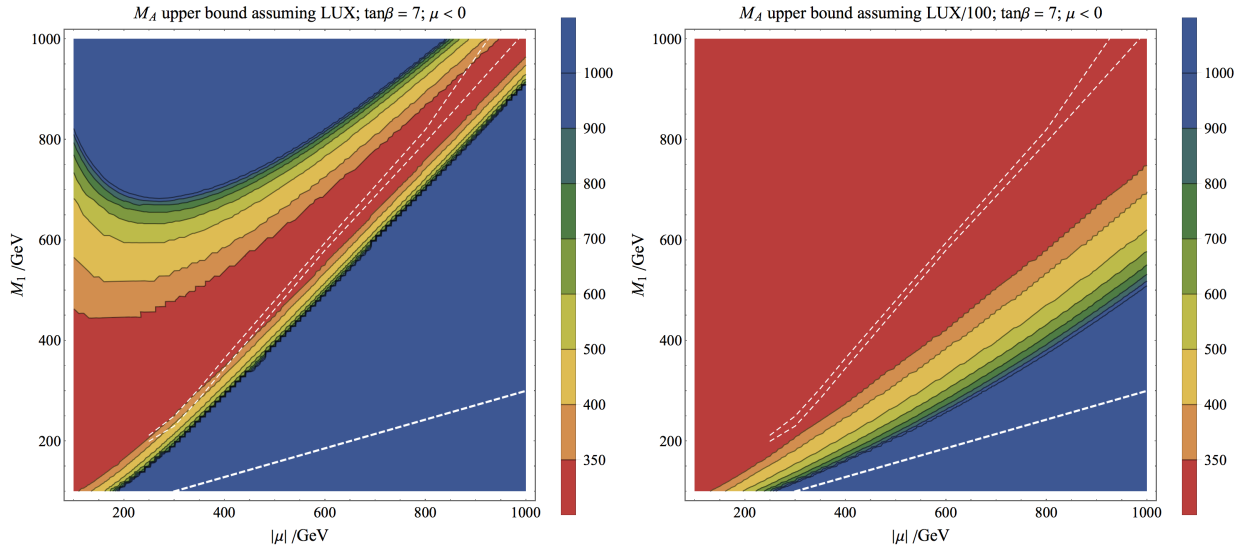
Figure. 3: Upper bounds on M_A due to 2016 LUX bounds and projected DDMD bounds 100 times stronger than LUX, respectively ($\mu < 0$), assuming the observed relic density in the whole parameter space. The value of M_A is chosen to be at the maximum value allowed by these bounds, and is indicated by the color scale. (Note that the color scheme differs from the previous plot such that the regions where the SI cross section is allowed as $M_A \rightarrow \infty$ is always shown in blue.) The region between the white dashed lines represents the well-tempered region. Under the strengthened bound a much larger portion of the $|\mu|-M_1$ plane is constrained. The dashed line below corresponds to where the left hand side of Eq. 6 is zero, corresponding to the vanishing of the neutralino coupling to the SM Higgs. Below this line the blind spot cannot be obtained since the left hand side of Eq. 6 becomes negative.

It is interesting to investigate the region to be probed by future DDMD experiments. In case of no detection, future experiments will push the experimental limits below the decoupled scattering cross section in greater regions of the $\mu - M_1$ plane. In particular, the projected bounds of the LZ experiment are approximately 100 times stronger than those from the LUX experiment [17]. Fig. 3 reveals that, assuming a dark matter density consistent with the observed one, these stronger bounds would constrain M_A in the entire region left of the well-tempered region, and in part of the region to the right as well. As before, if a thermal origin of the dark matter relic density is assumed, the well-tempered region may be achieved, but the upper bound on M_A would become smaller than about 300 GeV.

A more complete description of the exclusion state of the A-funnel region takes into account the upper bound on M_A presented above as well as the lower bound due to the overcompensation of the heavy CP-even Higgs contribution. As mentioned before, the region allowed by LUX and relic density considerations roughly correspond to the blue and dark green region in Fig. 3, where the required value for resonant annihilation $M_A \simeq 2M_1$ is below the upper bound set by LUX. (For $\mu > 0$, the correct relic density can be achieved near the
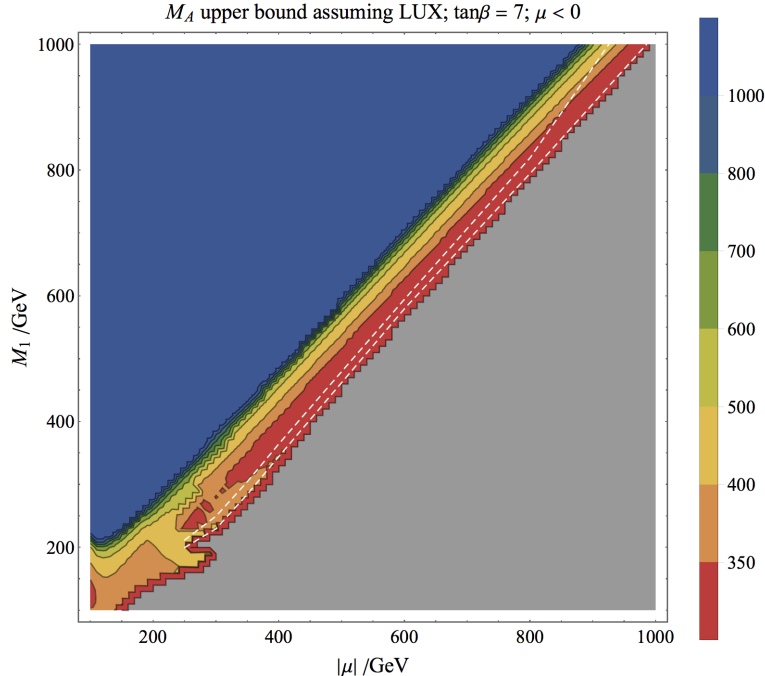
Figure. 4: Upper bounds on M_A due to 2016 LUX bounds, adjusted by the thermal WIMP relic density at each point in the plane. The strength of the LUX bound quickly decreases as one departs from the well-tempered region, since the WIMP relic density decrease quickly below the correct value. The gray region has relic density greater than 1.2 times the correct relic density, unless the neutralino mass is close to the resonant annihilation condition, $m_A = 2m_{\tilde{\chi}_1^0}$, for which the proper relic density may be obtained and the upper bound becomes the one shown in Fig. 3.

blue region of Fig. 2, where the required value is above the lower bound set by LUX.) The constraints from both sides are summarized in Fig. 5, which shows the exclusion states of the $|\mu|-M_1$ plane under present and projected DDMD constraints together with the relic density consideration. Below the viable well-tempered region, the exclusion states are determined by fixing M_A close to the resonant value $2m_{\tilde{\chi}_1^0}$ and comparing the SI cross section with the current and future bounds. The resulting bounds in this region combine the previous constraint on M_A away from the decoupling limit (upper bound) with the constraints from below. It can be seen that the present LUX bound leave the parameter space relatively open, while the projected (100 times strengthened) bound would considerably constrain the region in which resonant annihilation can be employed to obtain the correct relic density. In regions where the WIMP relic density is under-abundant, the upper bounds on M_A lifts up quickly if one adjust the LUX bound to match the WIMP relic density specific to each point in the $\mu - M_1$ plane, as shown in Fig. 4, opening up space for studies on mixed dark matter origin. We shall not concentrate on this scenario.
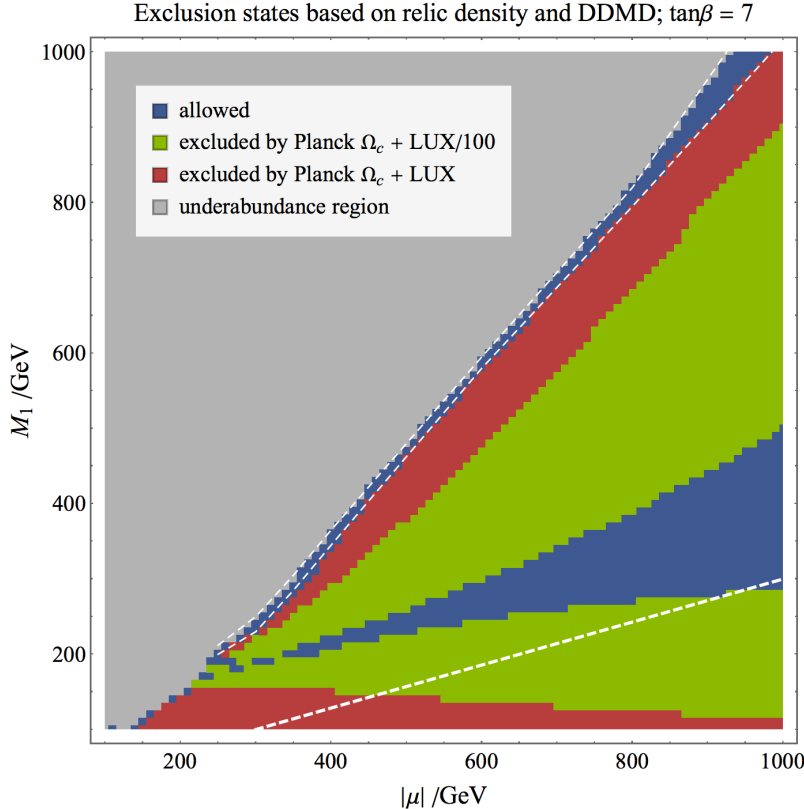
Figure. 5: Constraints on the $|\mu|-M_1$ plane under relic density constraints and the present and projected DDMD constraints. The well-tempered region ($\mu \simeq M_1$) naturally attains the correct relic density, while the region below may attain the correct value if M_A is tuned to mediate resonant annihilation. The required value of M_A is constrained by the LUX and 100 times strengthened LUX bound on SI cross section. The blue region is allowed by the 100 times strengthened LUX bound; the blue and the green regions are allowed under current LUX bound. Note that the boundaries of the LUX constraint (red) and of the LUX/100 constraint (green) above the blue region correspond to the boundaries in Fig. 3 where the upper bound on M_A is quickly lifted to infinity. The constraints below the blue region are due to the overcompensation in the scattering cross section from the heavy Higgs contribution.

B.   LZ Reach and Blind Spots

The lack of observation of a signal at the LZ experiment would constrain us to a narrow region of allowed parameter space for thermal dark matter, namely the A-funnel region displayed in Fig. 5, plus the well-tempered region for values of M_A consistent with the upper bound obtained in Fig. 3. The reach of LZ goes far beyond the natural values of the spin independent cross section for values of the gaugino and Higgsino masses of order of the weak scale, and therefore pushes the parameters towards the blind spot values. Alternatively, one could consider the event of an LZ detection of Dark Matter in the currently allowed range. In order to fix ideas and show the complementarity of different search methods in

detecting dark matter, we shall assume a detection of dark matter with a spin independent cross section of the order of $\sigma_p^{\text{SI}} = 10^{-11}$ pb, which is about 100 times lower than the LUX bound for $m_\chi = 500$ GeV, and within the sensitivity of the LZ experiments for WIMP masses 20 GeV$\lesssim m_\chi \lesssim 500$ GeV. Thus, for this range of WIMP masses, of order of the weak scale, future DDMD experiments will either detect dark matter or determine the proximity to the blind spot scenario, and probe it in such a case. Since, in addition, the blind spot scenario requires a specific correlation between the Higgs and neutralino masses, it can also be efficiently probed by spin dependent and indirect dark matter detection experiments, as well as by searches for Higgs and electroweakinos at the LHC.

The parameter space in which these small spin independent cross sections are achieved is well captured by the phenomenological MSSM (pMSSM) parameter space [35], but we have reduced its dimensionality to conduct a feasible study and to concentrate on critical variables. For instance, sfermion masses are held constant at 2 TeV, above experimental constraints, as they have little impact on the determination of the neutralino relic density and on DDMD experiments unless their masses are comparable to that of the LSP. By doing this, we are eliminating the interesting possibility of dark matter co-annihilation with scalar superpartners (see, for example, Refs. [36–40]), which is of phenomenological interest. We reserve the study of this case for future work.

In our analysis the trilinear coupling constants are fixed to be zero except for A_t , which is taken at a value of order 2 $M_S = 2\sqrt{M_{\tilde{t}_1} M_{\tilde{t}_2}}$ to obtain the proper 125 GeV Higgs mass [41–43]. The values of M_2 and M_3 are held well above M_1 so that the heavier electroweakinos do not interfere with the annihilation of the LSP. As mentioned before, we fixed $M_3 = 2$ TeV and chose M_2 by imposing the gaugino mass unification $M_2 = 2 M_1$ for simplicity, but our results are general whenever $M_2 \gtrsim 2 M_1$. As stressed before, the constraints on the parameter space become stronger for smaller values of M_2 and therefore we shall concentrate on the case of a Bino-like neutralino that leads to a larger allowed parameter space and also allows the obtention of a thermal relic density in larger regions of parameter space.

The four remaining parameters—$\tan\beta$, M_1, μ, and M_A —are critical to our model. For each combination of $\tan\beta$, M_1 and μ, we select M_A to obtain a cross section σ_p^{SI} smaller than the required bound on this quantity. In practice, as an example, we shall allow M_A to vary in the range consistent with $\sigma_p^{SI} \leq 10^{-11}$ pb. Hence, the boundaries of this region will be consistent with a potential measurement by LZ, while the central point would be close

to the parameters leading to the blind spot scenario. We shall focus our study on the region $5 \leq \tan \beta \leq 15$, that may accommodate the proper Higgs boson mass within the MSSM, and where our parameter space is left relatively open by the LHC $H \to \tau\tau$ and electroweakino (EWino) searches, and other collider constraints.

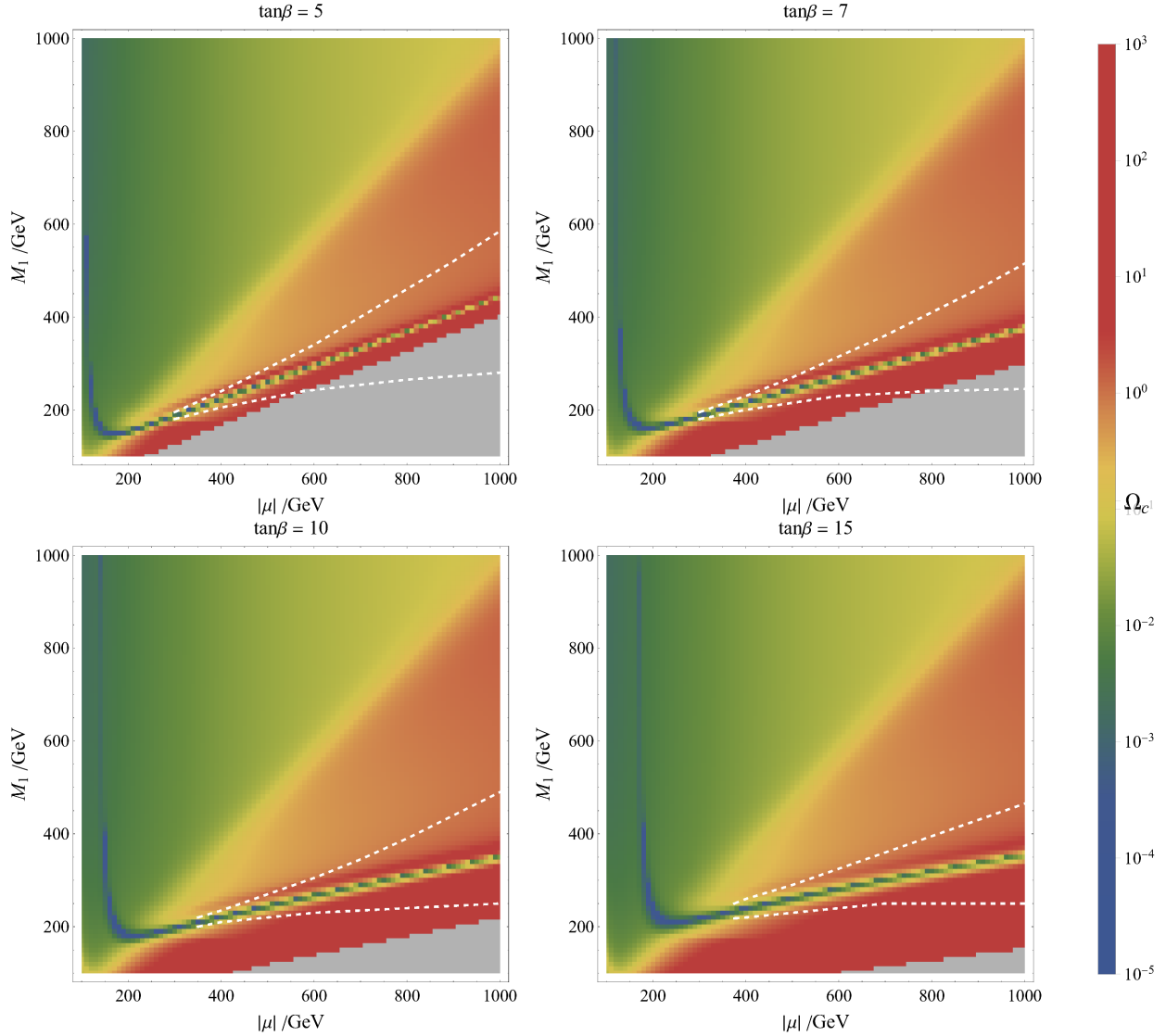Figure. 6: Thermal relic density shown in color on $|\mu|-M_1$ plane for various $\tan \beta$. M_A is taken to be at the center of blind spot (maximum cancellation). Note that μ is always negative for the blind spot to occur. The yellow region is consistent with the observed relic density. In the regions between the white dashed lines, M_A can be adjusted to mediate resonant annihilation while keeping $\sigma_p^{SI} < 10^{-11}$ pb. Blind spots are not achieved in the gray area since the left hand side of Eq. 6 becomes negative and destructive interference cannot happen. In this region, the $\sigma_p^{SI} < 10^{-11}$ pb requirement does not set an upper bound for M_A but only a lower bound, though it is still possible to tune M_A to achieve resonant annihilation for m_χ high enough.

We have used MicroOMEGAs (with SuSpect 2.41) to calculate the spectrum, SI and

SD DDMD cross sections and corresponding relic densities [44]. The thermal relic density is displayed on the $\mu - M_1$ plane in Fig. 6 for various values of $\tan\beta$, with M_A fixed at values consistent with the blind spot center (maximal destructive interference). The yellow color indicates that the region has the relic density consistent with the observed one [4, 29]. It can be clearly seen that the desired region consists of two branches: the well-tempered region $|\mu| \simeq M_1$ in the upper branch and the A-funnel region $|\mu| \simeq 2M_1$ in the lower branch. The resonant annihilation with the heavy Higgs is in fact so strong that the relic density rapidly decreases towards the center of the A-funnel region, so the correct relic density is only achieved on the two sides. However, since M_A is allowed to vary in a small range such that $\sigma_p^{SI} < 10^{-11}$ pb, the correct relic density can be attained in a wider region (between the white dashed lines in Fig. 6) by fine-tuning M_A. It can also be seen from Fig. 6 that both the well-tempered region and the A-funnel region in the blind spot scenario continues on almost linearly to $|\mu| \simeq 1$ TeV. These branches are approximated as piecewise linear functions when casting the collider constraints on the $\tan\beta - M_A$ plane in section IV.

IV   LHC Constraints

In this section we concentrate on the region of parameters consistent with $\sigma_p^{SI} \leq 10^{-11}$ pb. Recent LHC 13 TeV data reveals no signal of any BSM particles. The new exclusion limits from the ATLAS and CMS collaborations are used to constrain the parameter space of the blind spot scenario. In our region of interest where $\tan\beta$ is between 5 and 15, the $H, A \to \tau\tau$ searches [12, 45] offer the most stringent constraints. Electroweakino searches at CMS [46] provide additional constraints in the region of small M_1 and $|\mu|$, where $\widetilde{\chi}_1^0$ is especially light. In subsection A we examine constraints from the CMS and ATLAS $H, A \to \tau\tau$ searches, followed by an analysis of constraints from the $\widetilde{\chi}_2^0 \widetilde{\chi}_1^\pm \to WZ\widetilde{\chi}_1^0\widetilde{\chi}_1^0$ channel in subsection B. Overall, we find that the well-tempered region is completely excluded for $\tan\beta \geq 7$, and the A-funnel region is only partially excluded for the larger values of $\tan\beta$. The region of small $m_{\widetilde{\chi}_1^0}$ tends to be in tension with electroweakino searches.

A. $H \to \tau\tau$ Search

We consider production of the heavy Higgses H and A (either of which is denoted by ϕ) by means of gluon-gluon fusion ($gg\phi$) and b-associated production ($bb\phi$), followed by a decay into two τ leptons. Recent reports from CMS and ATLAS [12, 45] provide 2-dimensional 95% confidence level (CL) upper limits on parameters related to these decays. CMS puts bounds on $\sigma(gg\phi) \times BR(\phi \to \tau\tau)$ with respect to m_ϕ and $\sigma(bb\phi) \times BR(\phi \to \tau\tau)$, while ATLAS puts bounds on $\sigma_{\text{tot}} \times BR(\phi \to \tau\tau)$ with respect to m_ϕ and $f_b = \sigma(bb\phi)/\sigma_{\text{tot}}$. Their bounds are given for discrete M_A (and discrete f_b for ATLAS), so we linearly interpolate to find bounds at arbitrary values. While the CMS and ATLAS bounds consider the production and decay of either H or A, these processes are experimentally indistinguishable since $M_A \simeq M_H$ in our model, so we sum the cross section times branching ratio and compare these summed values to the experimental limits. We use FeynHiggs 2.12.0 [47–49] to compute the relevant cross sections and branching ratios for points in the blind spot scenario.

Piecewise linear approximations are made for M_1 as a function of $|\mu|$ in the well-tempered and A-funnel branches for $M_1, |\mu| > 200$ GeV, based on Fig. 6. We shall consider only $M_1, |\mu| \gtrsim 200$ GeV in this subsection, leaving an analysis of the $M_1, |\mu| \lesssim 200$ GeV case for subsections B and D. Cross sections and branching ratios are computed at points along these approximations with M_A chosen to be at the center of the blind spot, and are checked against the bounds in the ATLAS and CMS reports described above. The excluded regions in the $\tan\beta - M_A$ plane are shown in Fig. 7.

We see that at $\tan\beta = 6$ the well-tempered region is partially excluded, and for $\tan\beta \geq 7$ it is completely ruled out. Parts of the A-funnel region remain available at all $\tan\beta$, though the ATLAS results restrict large portions of parameter space for $\tan\beta > 10$. To reconcile Fig. 6 and Fig. 7, we present the exclusions in the $|\mu|-M_1$ plane for blind spots with the proper relic density in Fig. 8. The data set used in Fig. 8 is the same as for the yellow region in Fig. 6, so each data point has M_A chosen to be at the center of the blind spot, considering data points with the correct dark matter density. Again, we see that the well-tempered region is excluded for $\tan\beta \geq 7$, and the A-funnel region begins to be excluded as well as $\tan\beta$ increases. All data points shown in the A-funnel region are excluded by ATLAS for the $\tan\beta = 15$ plot, but the figure may be extended to reach allowed regions of parameters at higher $|\mu|$ and M_A. Fig. 8 also shows that M_A tends to be smaller in
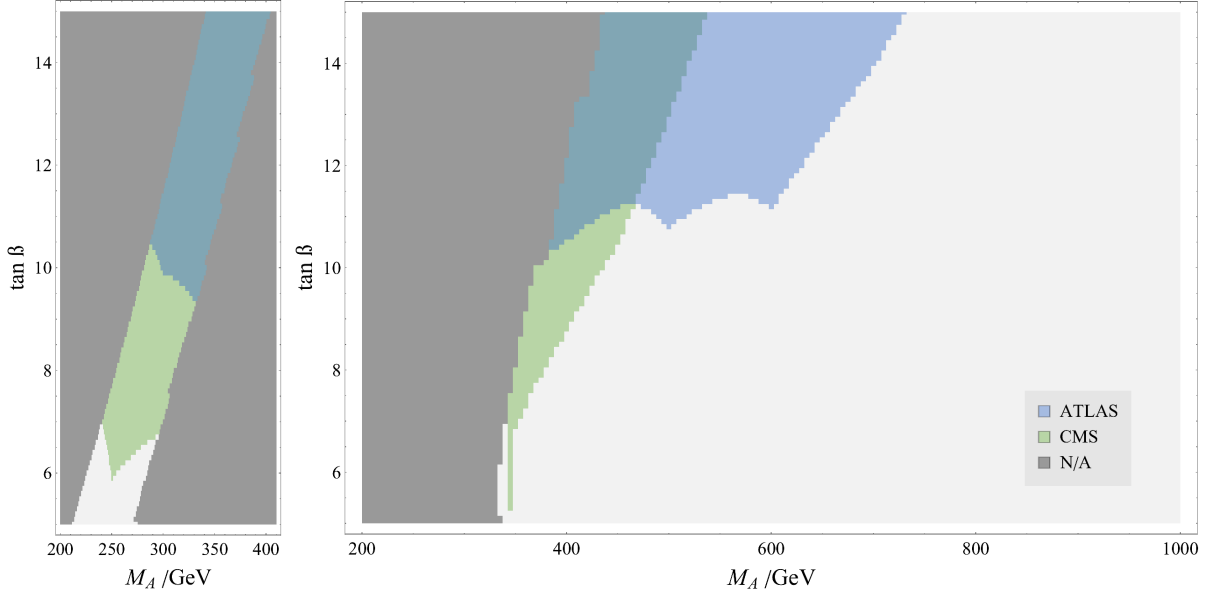
Figure. 7: Exclusion bounds on the well-tempered region and the A-funnel region in the $\tan\beta - M_A$ plane. The well-tempered region represented in the left panel and the A-funnel region in the right panel. The colored regions are excluded at 95% CL by the ATLAS or CMS results. The dark gray regions are not consistent with $\sigma_p^{SI} \leq 10^{-11}$ pb.

the well-tempered region, resulting in a higher production cross section, hence the greater degree of exclusion. On the other hand, as M_A increases in the A-funnel region, the $\phi \to \tau\tau$ branching ratio decreases as additional decay channels (notably the $\phi \to t\bar{t}$ channel) are opened and enhanced, resulting in a weaker exclusion limit.

We also investigate the effect of choosing M_A at the lower or upper limit consistent with $\sigma_p^{SI} = 10^{-11}$ pb on the exclusion status of our model. We survey the $|\mu|-M_A$ plane twice more, choosing M_A to be at the lower and upper limits. These new data are plotted in Fig. 9 and Fig. 10.

From Fig. 9 and Fig. 10 we see that, in the well-tempered region, the exclusion bounds are largely independent of which M_A we choose to achieve the $\sigma_p^{SI} \leq 10^{-11}$ pb condition. This stems from the fact that, in the well-tempered region, the variation of M_A from the values consistent with the blind spot scenario to the values leading to $\sigma_p^{SI} = 10^{-11}$ pb is $\Delta M_A \simeq 10 - 20$ GeV. Hence, the well-tempered region is still excluded for $\tan\beta \geq 7$. On the other hand, in the A-funnel region $\Delta M_A \simeq 100 - 300$ GeV for comparable points in Fig. 9 and Fig. 10, resulting in a greater disparity between exclusions in the $|\mu|-M_1$ plane, as is especially evident for the $\tan\beta = 15$ plots.
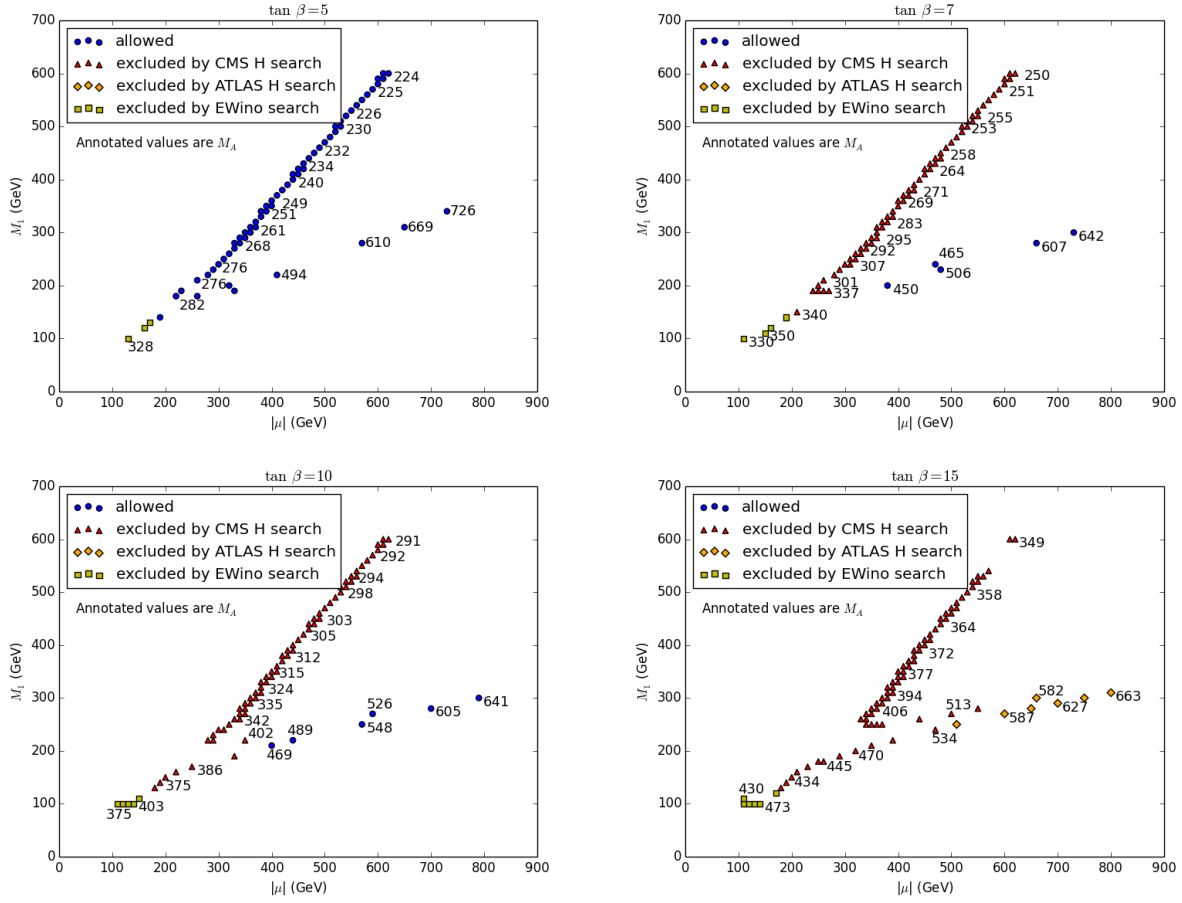
Figure. 8: Net exclusion status of the well-tempered region and the A-funnel region. Each data point represents a point with the proper relic density. Data points are first checked for exclusion by CMS, then by ATLAS, then by the CMS electroweakino searches (see the following section), with the color-coding of each data point corresponding to the method by which it is first excluded. Values of M_A are labeled next to selected data points. The sparseness of points in the A-funnel region reflects its narrowness relative to the well-tempered region, as seen in Fig. 6.

B.   Electroweakino Search

The $\phi \to \tau\tau$ searches leave open a small region of parameter space where M_A is sufficiently large to avoid these constraints, with $M_1, |\mu| < 200$ GeV. The neutralinos and charginos are light in this region, so electroweakino searches at LHC become relevant. The most stringent constraints are obtained from studying the decay products of the associated production of charginos and neutralinos, $\widetilde{\chi}_2^0 \widetilde{\chi}_1^\pm$. Since our slepton masses have been set high, the branching ratio for the decay of the second lightest neutralino and the lightest chargino $\widetilde{\chi}_2^0$, $\widetilde{\chi}_1^\pm$, into sleptons is negligible. In addition, since $m_{\widetilde{\chi}_2^0} \simeq m_{\widetilde{\chi}_1^\pm} < M_A + m_{\widetilde{\chi}_1^0}$, the decay of $\widetilde{\chi}_2^0$, $\widetilde{\chi}_1^\pm$ into heavy Higgs bosons is also negligible. This leaves $\widetilde{\chi}_2^0 \widetilde{\chi}_1^\pm \to WZ\widetilde{\chi}_1^0\widetilde{\chi}_1^0$ and $\widetilde{\chi}_2^0\widetilde{\chi}_1^\pm \to Wh\widetilde{\chi}_1^0\widetilde{\chi}_1^0$
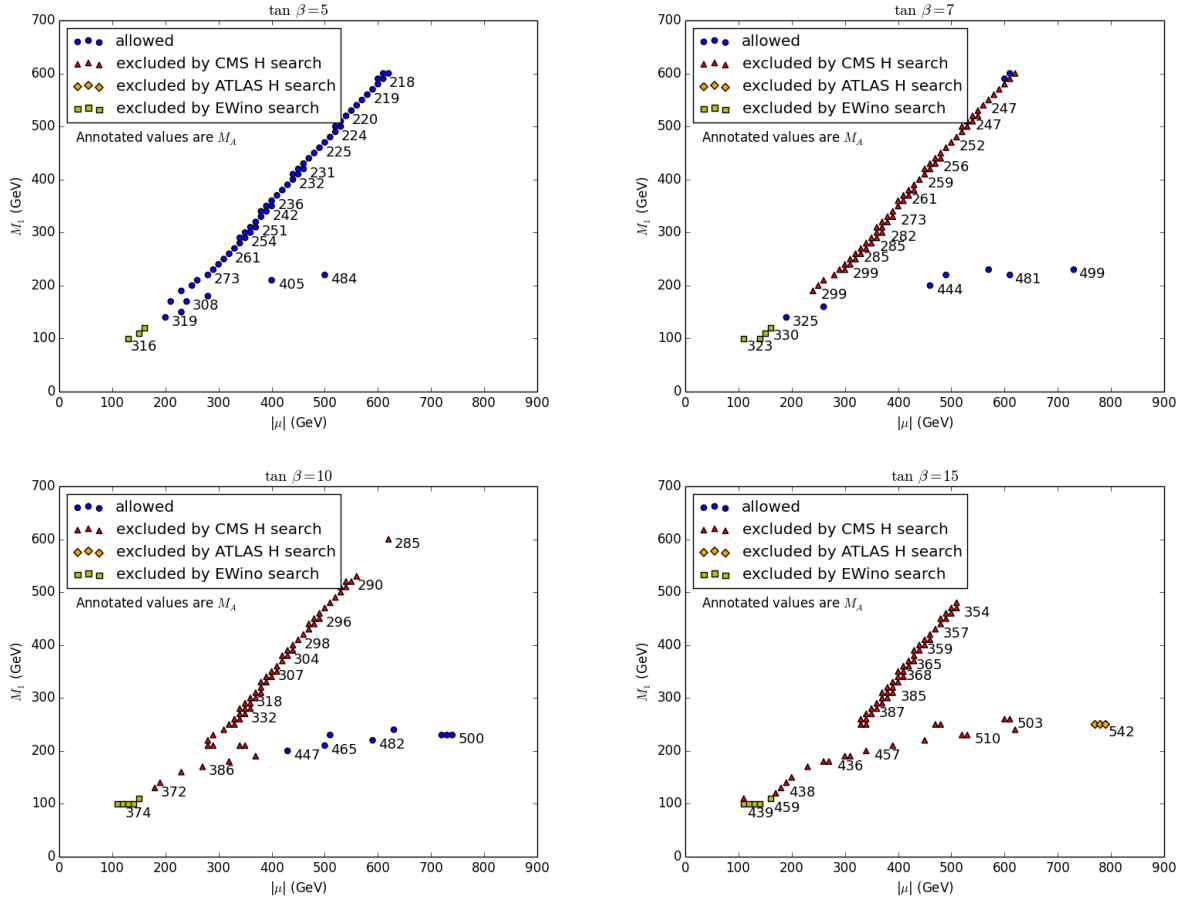
Figure. 9: Plot analogous to Fig. 8 with M_A chosen at the lower boundary consistent with $\sigma_p^{SI} = 10^{-11}$ pb . Only exclusions from the CMS $\phi \to \tau\tau$ search are shown.

as the only viable decay channels, with the final state containing a Z being the most sensitive one. In addition to the decay of $\widetilde{\chi}_2^0 \widetilde{\chi}_1^\pm$, the decay of $\widetilde{\chi}_3^0 \widetilde{\chi}_1^\pm$ is also a significant contributor to the $WZ\widetilde{\chi}_1^0\widetilde{\chi}_1^0$ final state. Production cross sections, computed with Prospino2 [50], for these and other electroweakino pairs are shown in Fig. 11. In the region of small M_1 and $|\mu|$, the masses of $\widetilde{\chi}_2^0$ and $\widetilde{\chi}_3^0$ are close, and thus the decays $\widetilde{\chi}_2^0\widetilde{\chi}_1^\pm \to WZ\widetilde{\chi}_1^0\widetilde{\chi}_1^0$ and $\widetilde{\chi}_3^0\widetilde{\chi}_1^\pm \to WZ\widetilde{\chi}_1^0\widetilde{\chi}_1^0$ are difficult to distinguish experimentally. Assuming this final state, CMS excludes a bounded region in the $m_{\widetilde{\chi}_1^0} - m_{\widetilde{\chi}_0^2}$ plane [46]. We exclude data points from the model according to the CMS bounds. To be more conservative in excluding points from the model, we use the mass $m_{\widetilde{\chi}_3^0}$ instead of $m_{\widetilde{\chi}_2^0}$ when testing points against the bounds in Ref. [46] A caveat to this method is that the CMS bounds assume wino-like $\widetilde{\chi}_2^0$ and $\widetilde{\chi}_1^\pm$, whereas for our data these electroweakinos are higgsino-like. The production cross sections for wino-like $\widetilde{\chi}_2^0\widetilde{\chi}_1^\pm$ are typically four times larger than those for higgsino-like electroweakinos
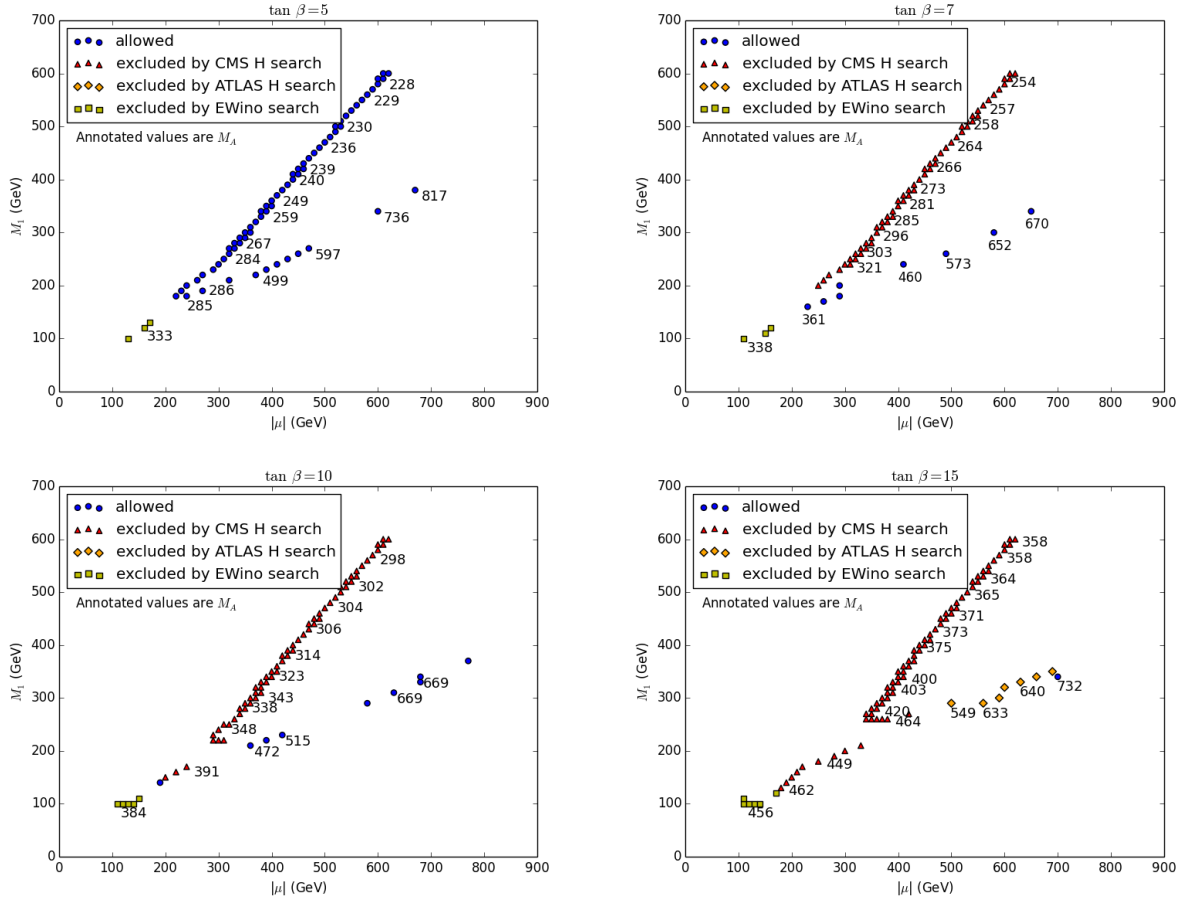
Figure. 10: Plot analogous to Fig. 8 with M_A chosen at the upper limit consistent with $\sigma_p^{SI} = 10^{-11}$ pb. Only exclusions from the CMS $\phi \to \tau\tau$ search are shown.

[51]. Even considering there are two higgsinos, the total higgsino production cross section is about half the wino production cross section, so the true bounds on our data are weaker than those presented in [46][1]. We find that these electroweakino searches do constrain this region, as shown by the yellow points in Figs. 8-10. Although the displayed bounds are generous for the Higgsino-like electroweakinos in our data, we will show in subsection D that this region of parameters is also excluded by recent IceCube results [53].

The High Luminosity-LHC would extend the scope of the electroweakino searches, and could probe up to 150 GeV to 600 GeV depending on the mass of the LSP [52, 54]. A 100 TeV collider can further extend the reach. For instance, when $m_{\tilde{\chi}_1^0}$ is below 500 GeV, a 100 TeV collider with 3 ab^{-1} can make a discovery of a higgsino on the order of 1.5 TeV in the

---

[1]For a recent analysis, see Ref [52]

trilepton channel [55]. In addition, in the well-tempered region, where $M_1 \sim |\mu|$, a future 100 TeV collider with 3 ab^{-1} can be sensitive to a mixed bino-higgsino LSP up to 1 TeV, and can reach 5σ discovery for $m_{\tilde{\chi}_1^0} \lesssim 165$ - 420 GeV depending on the mass difference between the two lightest neutralinos and the treatment of systematics [56].
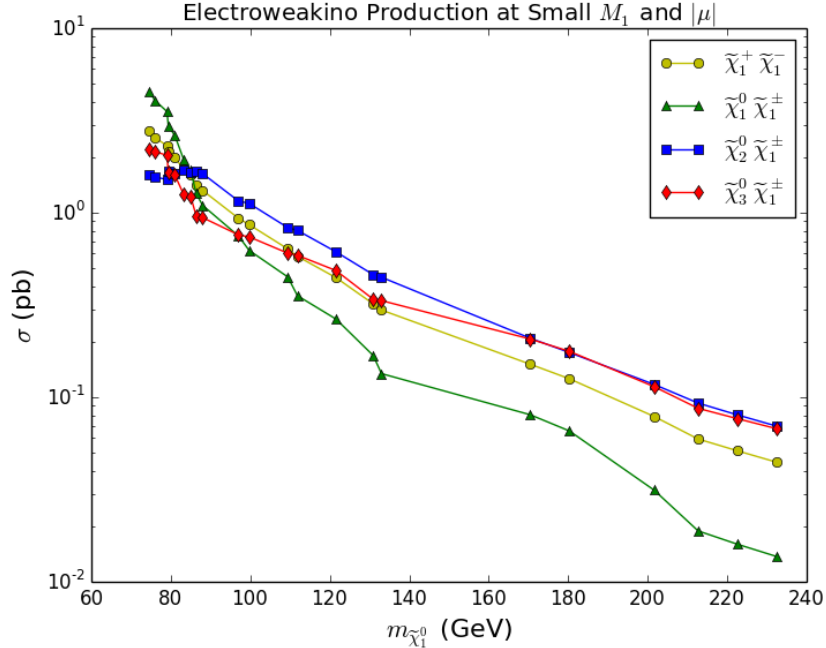

Figure. 11: Leading order cross sections for various electroweakino pair productions. Each data point corresponds to a blind spot with small M_1 and $|\mu|$ in the well-tempered region ($\mu \simeq M_1$) that was not excluded by the $\phi \to \tau\tau$ searches, although one outlier is not shown for the sake of readability. The plot incorporates points from all values of $\tan\beta$, since $\tan\beta$ does not have a significant effect on σ. For these data points $M_1 \simeq |\mu|$, and changes in the sign of $|\mu| - M_1$ can occur between data points. Thus the composition of the electroweakinos changes between data points as well. This results in bumps in the depicted curves since bino-like electroweakinos have lower cross sections than Higgsino-like electroweakinos of comparable mass.

C. Precision Higgs Measurements

In the well-tempered region, as M_A is light, there could be some tension with the precision Higgs data. At the tree level, the 125 GeV Higgs coupling to bottom-quarks in the MSSM is given by [57]

$$\frac{g_{hbb}}{g_{hbb}^{SM}} = -\frac{\sin\alpha}{\cos\beta} = \sin(\beta - \alpha) - \tan\beta\cos(\beta - \alpha). \tag{7}$$

The first term in the left-hand side of this expression, $\sin(\beta - \alpha)$, gives the ratio of the coupling of the Higgs to weak vector bosons to its SM value. In order to reproduce the

proper Higgs phenomenology, it should be close to one. Therefore, the corrections to the bottom coupling are controlled by the second term. One can work out an approximate expression for the value of this correction in the MSSM [58], at the one-loop level, namely

$$\tan\beta \, \cos(\beta - \alpha) \simeq \frac{-1}{m_H^2 - m_h^2} \left[m_h^2 - m_Z^2 \cos(2\beta) + \frac{3m_t^4 X_t(Y_t - X_t)}{4\pi^2 v^2 M_S^2} \left(1 - \frac{X_t^2}{6M_S^2} \right) \right] . \quad (8)$$

In the above, M_S is the average stop mass, $X_t = A_t - \mu/\tan\beta$, $Y_t = A_t + \mu\tan\beta$, A_t is the trilinear Higgs stop coupling and μ is the Higgsino mass parameter. The last term denotes the one-loop radiative corrections induced by the interaction of the Higgs bosons with the third generation squarks. At sizable values of $\tan\beta$ we can rewrite the above expression in the following approximate form,

$$\tan\beta \, \cos(\beta - \alpha) \simeq \frac{-1}{m_H^2 - m_h^2} \left[m_h^2 + m_Z^2 + \frac{3m_t^4}{4\pi^2 v^2 M_S^2} A_t\mu\tan\beta \left(1 - \frac{A_t^2}{6M_S^2} \right) \right] . \quad (9)$$

Since in order to obtain the proper Higgs mass in the MSSM the stop masses should be of the order of 1 TeV [41],[42],[43], and the value of $A_t < 3M_S$ due to vacuum stability constraints [59], it is clear that for the values of μ and $\tan\beta$ under consideration, the radiative corrections give only a small correction and the deviations of the bottom coupling from its SM value are well characterized by the first two terms inside the square bracket on the right-hand side of Eq. (9).

For instance, in the well-tempered region, when $\tan\beta$ is about 5, and the lightest neutralino is about 600 GeV, M_A is about 220 GeV as shown in Fig. 8. This leads to a bottom coupling that is about 70% higher than the SM value, which is about 4σ above the current central value and therefore ruled out by current Higgs precision measurements [45, 60]. We stress that this enhancement in the bottom coupling would lead to a large enhancement of the total width and therefore a suppression of the branching ratios of all other decay channels. In the region where M_A is larger, as approaching the decoupling limit, this tension is eased. For example, when $\tan\beta$ is about 5 and M_A is about 350 GeV, the bottom coupling to the Higgs is only about 20% higher than the SM, which corresponds to about two standard deviation of the experimental result (the current fit to the bottom Yukawa coupling shows a suppression of it [60][2]). Therefore, values of M_A larger than about 350 GeV are necessary

---

[2]The current fit also indicates an enhancement of the top Yukawa coupling. A suppression (enhancement) of the bottom (top) Yukawa coupling is difficult to achieve in the MSSM, but possible in the NMSSM [61, 62].

to be in agreement with precision electroweak data [45]. Such large values of M_A, however, are not consistent with the blind spot in the well-tempered region and therefore this MSSM scenario leads to tension with precision Higgs measurements.

The tension may be relaxed in two ways. Within the MSSM, one can consider the possibility of a SI DDMD cross section larger than the $\sigma_{SI} \simeq 10^{-11}$ pb assumed in this scenario. For instance, if we instead consider the maximal cross sections allowed by the current LUX bounds, as shown in Fig. 3, then the well-tempered region can coexist with the precision Higgs data for neutralino masses of order 300 GeV and heavy CP-even Higgs masses $m_H > 350$ GeV.

On the other hand, one can consider the possibility of extending the MSSM. In the simplest of such extensions, the NMSSM [63], in which a singlet superfield is added to the spectrum, the couplings and mixing of the CP-even Higgs bosons are modified by the appearance of new couplings and mixing with the singlet CP-even Higgs. In particular, the superpotential coupling λ of the singlet superfield to the Higgs doublets plays a significant role in defining the corrections to the bottom coupling to the lightest CP-even Higgs. If one considers the limit in which the singlet sector masses are raised by supersymmetry breaking terms, then the neutralino and Higgs boson particles in the low energy theory become identical as those ones in the MSSM. Moreover, one can consider the effective 2x2 CP-even Higgs mixing mass matrix after decoupling of the singlet fields, from where one can demonstrate that the bottom coupling has the same expression as in the MSSM, but the value of $\tan\beta \cos(\beta - \alpha)$ is now given by [64]

$$\tan\beta \, \cos(\beta - \alpha) \simeq \frac{-1}{m_H^2 - m_h^2} \left[m_h^2 + m_Z^2 - \lambda^2 v^2 + \frac{3m_t^4}{4\pi^2 v^2 M_S^2} A_t \mu \tan\beta \left(1 - \frac{A_t^2}{6M_S^2} \right) \right] . \quad (10)$$

From Eq. (10) it follows that for moderate or large values of $\tan\beta$, values of the coupling λ in the range $\lambda \simeq 0.6$–0.7 lead to small deviations of the bottom coupling with respect to the SM value, even for values of $m_H \simeq 200$ GeV. Hence, in the NMSSM, for heavy singlets and singlinos, the well-tempered region can be brought to agreement with precision Higgs measurements.

D. Spin-Dependent and Indirect Detection Constraints

Many direct and indirect detection experiments have also placed constraints on a DM particle interacting with a nucleus via spin dependent (SD) scattering. Spin dependent direct detection searches have been performed by the LUX [13] and XENON100 [15] experiments, but PICO [14] outperforms both of them. These exprimental results, however, do not set a strong bound on the regions of parameters explored in this paper. The exception comes from IceCube, which considers the detection of neutrinos coming from Dark Matter trapped and annihilating in the sun. The limits depend strongly on the annihilation channel but become strong for neutralinos annihilating into pairs of W^+W^- or ZZ gauge bosons [53], for which the current cross section limits are just below $\sigma_p^{SD} \simeq 10^{-4}$ pb. In our model, this annihilation channel is significant in the well-tempered neutralino region, where the higgsino component of the neutralino is largest and the Z boson coupling required for Z boson exchange in SD scattering is not suppressed. However, for 130 GeV $\lesssim m_{\tilde{\chi}_1^0} \lesssim 190$ GeV, the LSP also annihilates significantly into $b\bar{b}$, for which the IceCube bounds are weak. Furthermore, above 200 GeV the LSP begins annihilating into top quarks, and the branching ratio into W bosons diminishes. The remaining branching ratio is predominantly in the decay channels $ZH, W^\pm H^\mp$, and hA, which are not analyzed by IceCube. Assuming them to have bounds similar to the $t\bar{t}$ bounds, they will modify the constraints only slightly. Fig. 12 displays the branching ratios for these channels in the well-tempered region.

Figure 13 show the current 90% confidence level bounds on the blind spot scenarios coming from IceCube for the different values of $\tan\beta$ analyzed in this article. The lines labeled "IceCube combined" are the square roots of the harmonic means of σ_i^2 weighted by the branching ratios for our data, where i runs across the various decay channels. For the solid magenta line we have considered only the decays into W^+W^-, ZZ, and tt, rescaling the branching ratios to sum to one. In the dashed purple line we have included the decays $ZH, W^\pm H^\mp$, and hA, approximating them to make up the remainder of the branching ratio and have bounds on the similar to the $t\bar{t}$ bounds from IceCube. The latter method excludes dark matter masses in the well tempered region for $m_{\tilde{\chi}_1^0} \lesssim 200$ GeV, while the former method has a slightly stronger bound, excluding masses less than 210 GeV.

Finally, let us comment on indirect Dark Matter detection constraints. While the constraints from the Fermi experiment [65] do not affect the scenarios discussed in this article,
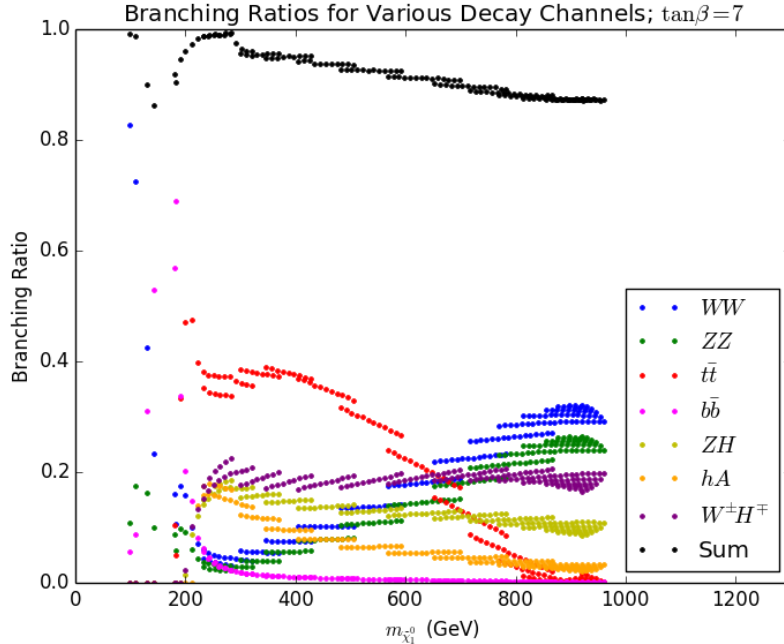
Figure. 12: Branching ratios for dark matter annihilation products, including W^+W^- (blue), ZZ (green), $t\bar{t}$ (red), $b\bar{b}$ (pink), ZH (yellow), hA (orange), $W^\pm H^\mp$ (purple), and their sum (black). We see that for $m_{\tilde{\chi}_1^0} < 200$ GeV, the W^+W^-, ZZ, and $b\bar{b}$ decay channels dominates. At $m_{\tilde{\chi}_1^0} \simeq 200$ GeV, the $t\bar{t}$ decay channel becomes prevalent, but begins to diminish for large $m_{\tilde{\chi}_1^0}$. For $m_{\tilde{\chi}_1^0} > 200$ GeV, the branching ratios for annihilation into W^+W^- and ZZ are similar, and the decays into ZH, hA, and $W^\pm H^\mp$ become significant.

there has been recent analyses of the AMS antiproton flux data [66] that claim strong constraints on thermal dark matter annihilating into bottom-quark pairs, with masses between 150 GeV and 450 GeV [67],[68]. Although there are large uncertainties having to do with propagation, solar modulation and antiproton production cross sections, if these bounds hold, the A-funnel region will be constrained to values of μ and M_A larger than about 1 TeV.

V   Conclusions

In this article we have studied the constraints and future probes of Dark Matter in the MSSM, in the case in which all scalar leptons and quarks are heavy. In particular, we have considered scenarios within the MSSM, in which the SI DDMD cross section is suppressed due to destructive interference between the light and heavy CP-even Higgs exchange amplitudes. We have shown that the proper relic density may be obtained in both the well-
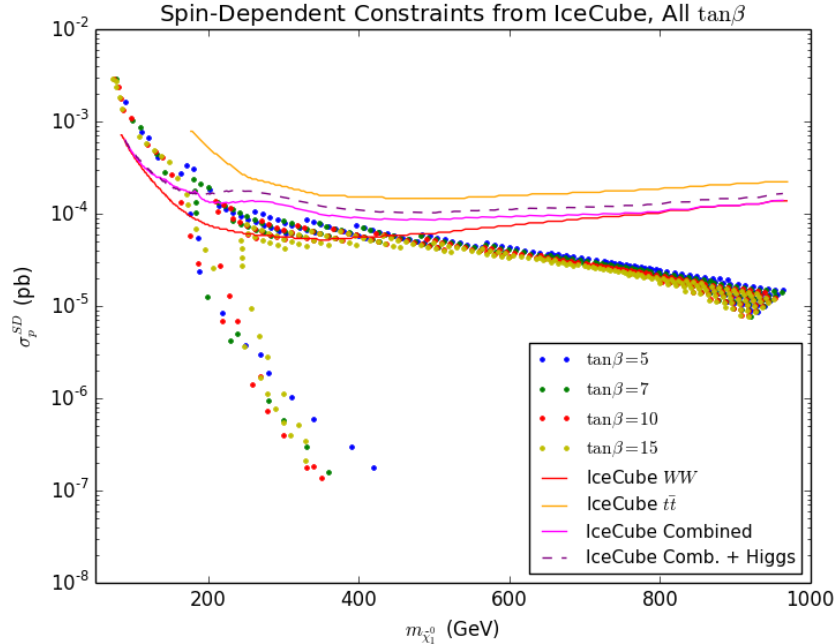
Figure. 13: Calculated spin dependent cross sections for $\tan\beta = 15$ (yellow dots), $\tan\beta = 10$ (red dots), $\tan\beta = 7$ (green dots) and $\tan\beta = 5$ (blue dots). The upper branch correspond to the well-tempered region, while the lower one corresponds to the A-funnel region. The red solid line represents the current 90% C.L. bound on the Spin dependent cross section coming from IceCube for annihilation into WW, and the orange line for annihilation into $t\bar{t}$. The bound for annihilation in to ZZ is very similar to the bound for annihilation into WW. The magenta and dashed purple lines combine these bounds, weighting them by the branching ratios for our data, with the dashed purple line further taking into account the decays into $ZH, W^{\pm}H^{\mp}$, and hA. The bounds for decay in $b\bar{b}$ are several orders of magnitude weaker and are not shown.

tempered neutralino region as well as in the A-funnel region. In the well-tempered region, the values of the heavy Higgs boson masses are lower than twice the top quark mass and this region of parameters may be efficiently probed by searches for production of heavy Higgs bosons decaying into τ-lepton pairs. Current searches already restrict the value of $\tan\beta < 7$ in this region of parameters and future searches can probe the whole region consistent with the blind spot scenario. Moreover, the IceCube are in tension with the well-tempered scenario for neutralino masses lower than 200 GeV. Furthermore, for neutralino masses larger than about 400 GeV, allowed values of the CP-odd Higgs mass may be in tension with those required to get consistency with precision Higgs measurements and the realization of this scenario may require a Higgs sector that goes beyond the MSSM one, like the one that is obtained in the NMSSM for heavy scalar and fermion singlets. Current bounds, however, allow the realization of the well-tempered scenario for neutralino masses of the order of 300 GeV, $\tan\beta \simeq 5$ and heavy Higgs bosons of about 400 GeV.

In the A-funnel region, the heavy Higgs boson masses are larger and, therefore, this region of parameters cannot be fully probed by current or future LHC searches for heavy Higgs bosons. This is particularly true at lower values of $\tan\beta$, where the decay into top-quark pairs tends to be comparable or larger than the one into τ-lepton pairs. On the other hand, electroweakino searches present an alternative way of probing this scenario, although it is efficient only for low values of μ and M_1. Finally, for values of the neutralino mass lower than 450 GeV, this region of parameters may be in tension with recent AMS antiproton data, what may require to go to values of M_A and μ larger than about 1 TeV.

Acknowledgements

---

[1] F. Zwicky, "On the Masses of Nebulae and of Clusters of Nebulae," *Astrophys. J.* **86** (Oct., 1937) 217.

[2] A. Bosma, "21-cm line studies of spiral galaxies. ii. the distribution and kinematics of neutral hydrogen in spiral galaxies of various morphological types," *Astronomical Journal* **86** (1981) 1825 – 1846. `http://adsabs.harvard.edu/cgi-bin/bib_query?1981AJ.....86.1825B`.

[3] K. Begeman, A. Broeils, and R. Sanders, "Extendend rotation curves of spiral galaxies: dark haloes and modified dynamics," *Monthly Notices of the Royal Astronomical Society* **249** (1991) 523–537. `http://adsabs.harvard.edu/abs/1991MNRAS.249..523B`.

[4] **Planck** Collaboration, P. A. R. Ade *et al.*, "Planck 2015 results. XIII. Cosmological parameters," *Astron. Astrophys.* **594** (2016) A13, `arXiv:1502.01589 [astro-ph.CO]`.

[5] M. Kamionkowski, "WIMP and axion dark matter," in *High-energy physics and cosmology.*

Proceedings, Summer School, Trieste, Italy, June 2-July 4, 1997, pp. 394–411. 1997.
`arXiv:hep-ph/9710467 [hep-ph]`.

`http://alice.cern.ch/format/showfull?sysnb=0260730`.

[6] G. Jungman, M. Kamionkowski, and K. Griest, "Supersymmetric dark matter," *Phys. Rept.*
267 (1996) 195–373, `arXiv:hep-ph/9506380 [hep-ph]`.

[7] **ATLAS** Collaboration, M. Aaboud *et al.*, "Search for squarks and gluinos in events with
hadronically decaying tau leptons, jets and missing transverse momentum in proton-proton
collisions at $\sqrt{s} = 13$ TeV recorded with the ATLAS detector," `arXiv:1607.05979`
`[hep-ex]`.

[8] **CMS** Collaboration, C. Collaboration, "Exclusion limits on gluino and top-squark pair
production in natural SUSY scenarios with inclusive razor and exclusive single-lepton
searches at 8 TeV.,".

[9] **ATLAS** Collaboration, G. Aad *et al.*, "Search for direct production of charginos,
neutralinos and sleptons in final states with two leptons and missing transverse momentum
in *pp* collisions at $\sqrt{s} = 8$ TeV with the ATLAS detector," *JHEP* **05** (2014) 071,
`arXiv:1403.5294 [hep-ex]`.

[10] **CMS** Collaboration, V. Khachatryan *et al.*, "Searches for electroweak neutralino and
chargino production in channels with Higgs, Z, and W bosons in pp collisions at 8 TeV,"
Phys. Rev. **D90** no. 9, (2014) 092007, `arXiv:1409.3168 [hep-ex]`.

[11] **DELPHI** Collaboration, J. Abdallah *et al.*, "Searches for supersymmetric particles in e+ e-
collisions up to 208-GeV and interpretation of the results within the MSSM," *Eur. Phys. J.*
C31 (2003) 421–479, `arXiv:hep-ex/0311019 [hep-ex]`.

[12] **CMS Collaboration** Collaboration, "Search for a neutral mssm higgs boson decaying into
tautau at 13 tev," Tech. Rep. CMS-PAS-HIG-16-006, CERN, Geneva, 2016.

[13] **LUX** Collaboration, D. S. Akerib *et al.*, "Results from a search for dark matter in the
complete LUX exposure," `arXiv:1608.07648v2 [astro-ph.CO]`.

[14] **PICO Collaboration** Collaboration, "Dark matter search results from the pico-60 cf_3I
bubble chamber," *Phys. Rev. D* **93** (Mar, 2016) 052014.
`http://link.aps.org/doi/10.1103/PhysRevD.93.052014`.

[15] **XENON100** Collaboration, E. Aprile *et al.*, "Dark Matter Results from 225 Live Days of
XENON100 Data," *Phys. Rev. Lett.* **109** (2012) 181301, `arXiv:1207.5988 [astro-ph.CO]`.

[16] **PandaX-II** Collaboration, A. Tan *et al.*, "Dark Matter Results from First 98.7-day Data of PandaX-II Experiment," *Phys. Rev. Lett.* **117** no. 12, (2016) 121303, `arXiv:1607.07400 [hep-ex]`.

[17] **LZ** Collaboration, D. S. Akerib *et al.*, "LUX-ZEPLIN (LZ) Conceptual Design Report," `arXiv:1509.02910 [physics.ins-det]`.

[18] **XENON1T collaboration** Collaboration, E. Aprile, "The XENON1T Dark Matter Search Experiment," `arXiv:1206.6288 [astro-ph.IM]`.

[19] C. Cheung, L. J. Hall, D. Pinner, and J. T. Ruderman, "Prospects and Blind Spots for Neutralino Dark Matter," *JHEP* **1305** (2013) 100, `arXiv:1211.4873 [hep-ph]`.

[20] V. Mandic, A. Pierce, P. Gondolo, and H. Murayama, "The Lower bound on the neutralino nucleon cross-section," `arXiv:hep-ph/0008022 [hep-ph]`.

[21] J. R. Ellis, A. Ferstl, and K. A. Olive, "Reevaluation of the elastic scattering of supersymmetric dark matter," *Phys.Lett.* **B481** (2000) 304–314, `arXiv:hep-ph/0001005 [hep-ph]`.

[22] J. Ellis, A. Ferstl, and K. A. Olive, "Exploration of elastic scattering rates for supersymmetric dark matter," *Phys. Rev. D* **63** (Feb, 2001) 065016. `http://link.aps.org/doi/10.1103/PhysRevD.63.065016`.

[23] J. R. Ellis, K. A. Olive, Y. Santoso, and V. C. Spanos, "Update on the direct detection of supersymmetric dark matter," *Phys.Rev.* **D71** (2005) 095007, `arXiv:hep-ph/0502001 [hep-ph]`.

[24] H. Baer, A. Mustafayev, E.-K. Park, and X. Tata, "Target dark matter detection rates in models with a well-tempered neutralino," *JCAP* **0701** (2007) 017, `arXiv:hep-ph/0611387 [hep-ph]`.

[25] T. Han, Z. Liu, and S. Su, "Light Neutralino Dark Matter: Direct/Indirect Detection and Collider Searches," *JHEP* **08** (2014) 093, `arXiv:1406.1181 [hep-ph]`.

[26] H. Baer, V. Barger, P. Huang, D. Mickelson, M. Padeffke-Kirkland, and X. Tata, "Natural SUSY with a bino- or wino-like LSP," *Phys. Rev.* **D91** no. 7, (2015) 075005, `arXiv:1501.06357 [hep-ph]`.

[27] P. Huang and C. E. M. Wagner, "Blind Spots for neutralino Dark Matter in the MSSM with an intermediate m˙A," *Phys. Rev.* **D90** no. 1, (2014) 015018, `arXiv:1404.0392 [hep-ph]`.

[28] N. Arkani-Hamed, A. Delgado, and G. Giudice, "The Well-tempered neutralino," *Nucl.Phys.*

B741 (2006) 108–130, `arXiv:hep-ph/0601041 [hep-ph]`.

[29] **WMAP** Collaboration, G. Hinshaw *et al.*, "Nine-Year Wilkinson Microwave Anisotropy Probe (WMAP) Observations: Cosmological Parameter Results," *Astrophys.J.Suppl.* **208** (2013) 19, `arXiv:1212.5226 [astro-ph.CO]`.

[30] J. Bramante, N. Desai, P. Fox, A. Martin, B. Ostdiek, and T. Plehn, "Towards the Final Word on Neutralino Dark Matter," *Phys. Rev.* **D93** no. 6, (2016) 063525, `arXiv:1510.03460 [hep-ph]`.

[31] R. J. Hill and M. P. Solon, "Universal behavior in the scattering of heavy, weakly interacting dark matter on nuclear targets," *Phys.Lett.* **B707** (2012) 539–545, `arXiv:1111.0016 [hep-ph]`.

[32] E. Bagnaschi *et al.*, "Likelihood Analysis of the Minimal AMSB Model," `arXiv:1612.05210 [hep-ph]`.

[33] G. B. Gelmini and P. Gondolo, "Neutralino with the right cold dark matter abundance in (almost) any supersymmetric model," *Phys. Rev.* **D74** (2006) 023510, `arXiv:hep-ph/0602230 [hep-ph]`.

[34] H. Baer, V. Barger, and H. Serce, "SUSY under siege from direct and indirect WIMP detection experiments," `arXiv:1609.06735 [hep-ph]`.

[35] **MSSM Working Group** Collaboration, A. Djouadi *et al.*, "The Minimal supersymmetric standard model: Group summary report," in *GDR (Groupement De Recherche) - Supersymetrie Montpellier, France, April 15-17, 1998.* 1998. `arXiv:hep-ph/9901246 [hep-ph]. https://inspirehep.net/record/481987/files/arXiv:hep-ph_9901246.pdf`.

[36] J. R. Ellis, T. Falk, K. A. Olive, and M. Srednicki, "Calculations of neutralino-stau coannihilation channels and the cosmologically relevant region of MSSM parameter space," *Astropart. Phys.* **13** (2000) 181–213, `arXiv:hep-ph/9905481 [hep-ph]`. [Erratum: Astropart. Phys.15,413(2001)].

[37] C. Balazs, M. Carena, and C. E. M. Wagner, "Dark matter, light stops and electroweak baryogenesis," *Phys. Rev.* **D70** (2004) 015007, `arXiv:hep-ph/0403224 [hep-ph]`.

[38] J. R. Ellis, K. A. Olive, and Y. Santoso, "Calculations of neutralino stop coannihilation in the CMSSM," *Astropart. Phys.* **18** (2003) 395–432, `arXiv:hep-ph/0112113 [hep-ph]`.

[39] M. A. Ajaib, T. Li, and Q. Shafi, "Stop-Neutralino Coannihilation in the Light of LHC,"

Phys. Rev. **D85** (2012) 055021, `arXiv:1111.4467 [hep-ph]`.

[40] A. Ibarra, A. Pierce, N. R. Shah, and S. Vogl, "Anatomy of Coannihilation with a Scalar Top Partner," *Phys. Rev.* **D91** no. 9, (2015) 095018, `arXiv:1501.03164 [hep-ph]`.

[41] P. Draper, G. Lee, and C. E. M. Wagner, "Precise estimates of the Higgs mass in heavy supersymmetry," *Phys. Rev.* **D89** no. 5, (2014) 055023, `arXiv:1312.5743 [hep-ph]`.

[42] J. Pardo Vega and G. Villadoro, "SusyHD: Higgs mass Determination in Supersymmetry," *JHEP* **07** (2015) 159, `arXiv:1504.05200 [hep-ph]`.

[43] G. Lee and C. E. M. Wagner, "Higgs bosons in heavy supersymmetry with an intermediate m_A," *Phys. Rev.* **D92** no. 7, (2015) 075032, `arXiv:1508.00576 [hep-ph]`.

[44] G. Bélanger, F. Boudjema, A. Pukhov, and A. Semenov, "Micromegas4. 1: two dark matter candidates," *Computer Physics Communications* **192** (2015) 322–329.

[45] **ATLAS Collaboration** Collaboration, "Search for minimal supersymmetric standard model higgs boson h/a in the tautau final state in up to 13.3/fb of pp collisions at sqrt(s) = 13 tev with the atlas detector," Tech. Rep. ATLAS-CONF-2016-085, CERN, Geneva, Aug, 2016.

[46] **CMS Collaboration** Collaboration, "Search for electroweak susy production in multilepton final states in pp collisions at sqrt(s) = 13 tev with 12.9/fb," Tech. Rep. CMS-PAS-SUS-16-024, CERN, Geneva, 2016.

[47] H. Bahl and W. Hollik, "Precise prediction for the light mssm higgs boson mass combining effective field theory and fixed-order calculations," `arXiv:1608.01880 [hep-ph]`.

[48] T. Hahn, S. Heinemeyer, W. Hollik, H. Rzehak, and G. Weiglein, "High-precision predictions for the light cp-even higgs boson mass of the mssm," *Phys. Rev. Lett.* **112** (2014) , `arXiv:1312.4937 [hep-ph]`.

[49] S. Heinemeyer, W. Hollik, and G. Weiglein, "Feynhiggs: a program for the calculation of the masses of the neutral cp-even higgs bosons in the mssm," *Comput. Phys. Commun.* **124** (2000) 76–89, `arXiv:9812320 [hep-ph]`.

[50] W. Beenakker, R. Hopker, and M. Spira, "PROSPINO: A Program for the production of supersymmetric particles in next-to-leading order QCD," `arXiv:hep-ph/9611232 [hep-ph]`.

[51] C. Borschenksy *et al.*, "Square and gluino production cross sections in pp collisions at sqrt(s) = 13, 14, 33 and 100 tev," Tech. Rep. CERN-PH-TH-2014-137, MS-TP-14-25, TTK-14-13, CERN, 2014. `arXiv:1407.5066v2 [hep-ph]`.

[52] T. Han, F. Kling, S. Su, and Y. Wu, "Unblind the Dark Matter Blind Spots," *Submitted to: JHEP* (2016) , `arXiv:1612.02387 [hep-ph]`.

[53] **IceCube** Collaboration, M. G. Aartsen *et al.*, "Improved limits on dark matter annihilation in the Sun with the 79-string IceCube detector and implications for supersymmetry," *JCAP* **1604** no. 04, (2016) 022, `arXiv:1601.00653 [hep-ph]`.

[54] **CMS** Collaboration, "Projected Performance of an Upgraded CMS Detector at the LHC and HL-LHC: Contribution to the Snowmass Process," in *Proceedings, Community Summer Study 2013: Snowmass on the Mississippi (CSS2013): Minneapolis, MN, USA, July 29-August 6, 2013.* 2013. `arXiv:1307.7135 [hep-ex]`. `https://inspirehep.net/record/1244669/files/arXiv:1307.7135.pdf`.

[55] S. Gori, S. Jung, L.-T. Wang, and J. D. Wells, "Prospects for Electroweakino Discovery at a 100 TeV Hadron Collider," *JHEP* **12** (2014) 108, `arXiv:1410.6287 [hep-ph]`.

[56] M. Low and L.-T. Wang, "Neutralino dark matter at 14 TeV and 100 TeV," *JHEP* **08** (2014) 161, `arXiv:1404.0682 [hep-ph]`.

[57] J. F. Gunion and H. E. Haber, "Higgs Bosons in Supersymmetric Models. 1.," *Nucl. Phys.* **B272** (1986) 1. [Erratum: Nucl. Phys.B402,567(1993)].

[58] M. Carena, H. E. Haber, I. Low, N. R. Shah, and C. E. M. Wagner, "Complementarity between Nonstandard Higgs Boson Searches and Precision Higgs Boson Measurements in the MSSM," *Phys. Rev.* **D91** no. 3, (2015) 035003, `arXiv:1410.4969 [hep-ph]`.

[59] N. Blinov and D. E. Morrissey, "Vacuum Stability and the MSSM Higgs Mass," *JHEP* **03** (2014) 106, `arXiv:1310.4174 [hep-ph]`.

[60] **ATLAS, CMS** Collaboration, G. Aad *et al.*, "Measurements of the Higgs boson production and decay rates and constraints on its couplings from a combined ATLAS and CMS analysis of the LHC pp collision data at $\sqrt{s} = 7$ and 8 TeV," *JHEP* **08** (2016) 045, `arXiv:1606.02266 [hep-ex]`.

[61] M. Badziak and C. E. M. Wagner, "Enhancing the Higgs associated production with a top quark pair," *JHEP* **05** (2016) 123, `arXiv:1602.06198 [hep-ph]`.

[62] M. Badziak and C. E. M. Wagner, "Enhanced Higgs associated production with a top quark pair in the NMSSM with light singlets," `arXiv:1611.02353 [hep-ph]`.

[63] U. Ellwanger, C. Hugonie, and A. M. Teixeira, "The Next-to-Minimal Supersymmetric Standard Model," *Phys. Rept.* **496** (2010) 1–77, `arXiv:0910.1785 [hep-ph]`.

[64] M. Carena, H. E. Haber, I. Low, N. R. Shah, and C. E. M. Wagner, "Alignment limit of the NMSSM Higgs sector," *Phys. Rev.* **D93** no. 3, (2016) 035013, `arXiv:1510.09137 [hep-ph]`.

[65] **Fermi-LAT** Collaboration, M. Ackermann *et al.*, "Searching for Dark Matter Annihilation from Milky Way Dwarf Spheroidal Galaxies with Six Years of Fermi Large Area Telescope Data," *Phys. Rev. Lett.* **115** no. 23, (2015) 231301, `arXiv:1503.02641 [astro-ph.HE]`.

[66] **AMS** Collaboration, M. Aguilar *et al.*, "Antiproton Flux, Antiproton-to-Proton Flux Ratio, and Properties of Elementary Particle Fluxes in Primary Cosmic Rays Measured with the Alpha Magnetic Spectrometer on the International Space Station," *Phys. Rev. Lett.* **117** no. 9, (2016) 091103.

[67] A. Cuoco, M. Krmer, and M. Korsmeier, "Novel dark matter constraints from antiprotons in the light of AMS-02," `arXiv:1610.03071 [astro-ph.HE]`.

[68] M.-Y. Cui, Q. Yuan, Y.-L. S. Tsai, and Y.-Z. Fan, "A possible dark matter annihilation signal in the AMS-02 antiproton data," `arXiv:1610.03840 [astro-ph.HE]`.